Coordinated downregulation of the photosynthetic apparatus as a protective mechanism against UV exposure in the diatom *Corethron hystrix*

Robert W. Read[1], David C. Vuono[1], Iva Neveux[1], Carl Staub[2] and Joseph J. Grzymski[1]

1. Division of Earth and Ecosystem Sciences, Desert Research Institute, Reno, NV 89512, USA

2. Agtron, Inc. 9395 Double R Blvd, Reno, NV 89521, USA

Correspondence: Joseph J. Grzymski, Department of Earth and Ecosystem Sciences, Desert Research Institute, 2215 Raggio Parkway, Reno, NV 89509, USA.

***E-mail: joeg@dri.edu**

Abstract:

The effect of ultraviolet radiation (UVR) on photosynthetic efficiency and the resulting mechanisms against UV exposure employed by phytoplankton are not completely understood. To address this knowledge gap, we developed a novel close-coupled, wavelength-configurable platform designed to produce precise and repeatable *in vitro* irradiation of *Corethron hystrix*, a member of a genera found abundantly in the Southern Ocean where UV exposure is high. We aimed to determine its metabolic, protective, mutative, and repair mechanisms as a function of varying levels of specific electromagnetic energy. Our results show that the physiological responses to each energy level of UV have a negative linear decrease in the photosynthetic efficiency of photosystem II proportional to UV intensity, corresponding to a large increase in the turnover time of quinone re-oxidation. Gene expression changes of photosystem II related reaction center proteins D1, CP43 and CP47 showed coordinated downregulation whereas the central metabolic pathway demonstrated mixed expression of up and downregulated transcripts after UVR exposure. These results suggest that while UVR may damage photosynthetic machinery, oxidative damage may limit production of new photosynthetic and electron transport complexes as a result of UVR exposure.

Keywords: Diatom, UVR, Photosynthetic damage, Transcriptome

Introduction:

Diatoms are microscopic photosynthetic algae that are ubiquitous throughout the surface waters of the oceans (Lohman 1960), account for roughly 40% of oceanic primary production, and one-fifth of the Earth's total primary production (Falkowski and Raven 2007). Diatoms also play a vital role in the global carbon cycle through their uptake of dissolved CO_2 and subsequent carbon fixation that forms the base of the marine food web (Armbrust 2009). Given their global distribution, diatoms have adapted to survive under a variety of environmental conditions (Ligowski et al. 2012; Verde and Prisco 2012; Marchetti et al. 2012). Unfavorable conditions such as nutrient limitation (Allen et al. 2008; Dyhrman et al. 2012; Shrestha et al. 2012; Bender et al. 2014), varying light levels (Domingues et al. 2012; Herbstová et al. 2015) and UV exposure (Wu et al. 2015) are commonplace. The latter is of particular interest because of the damaging effects UV can have on photosynthesis as well as other metabolic pathways.

In phytoplankton, UV exposure can inhibit photosynthesis, based on the relative dose and dose rate (Cullen and Lesser 1991). An inhibition of the photosynthetic rate causes a decrease in the rate of primary production, with consequences in marine ecosystems as well as terrestrial environments. Phytoplankton can also produce protective compounds to combat the deleterious effects of UVR such as mycosporine-like amino acids (MAAs), DNA photolyases and many more undefined compounds (Helbling et al. 1996; Coesel et al. 2009). These compounds, when added to commercial products such as sunscreen (Berardesca et al. 2012; Emanuele et al. 2013), show promise in reducing carcinogenic effects of UV exposure in humans. Advances in this field require a reliable method to induce and measure damage in a controlled laboratory setting.

Fluorescence kinetics measurements are a reliable estimator of photosynthetic electron transport rates and photosystem II health (PSII) (Kolber and Falkowski 1993) in photoautotrophic organisms. Because PSII is a target of UVR induced damage (Tevini and Teramura 1989; Szilárd et al. 2007), Fast Repetition Rate Fluorometry (FRRF) has been used to examine variations in several photosynthetic parameters in relation to light impacts on the cell (Kolber et al. 1998). Changes in parameters such as the maximum quantum yield of PSII (Fv/Fm) (Geider et al. 1993; Kolber and Falkowski 1993), the turnover time of electron transport from QA -> QB (tau1) and QB -> PQ (tau2) (Kolber et al. 1988), and the functional cross section of PSII (σ_{PSII}) -- the effective target size of the PSII antenna in $Å^2$ $(quanta)^{-1}$ (Kolber et al. 1998), act as proxies to monitor electron transport rates and the relative health of PSII. Here we use them to monitor the rate and intensity of photosynthetic damage within the cell. Changes in these parameters are a function of the dose and dosage rate of absorbed radiation, as this has a direct impact of the oxidation state of PSII electron transport chain.

In this study, the diatom *C. hystrix* (CCMP 308) was subjected to increasing intensities of UVR energy ranging from 0.32 mW/cm^2 to 1.59 mW/cm^2 using a custom built UVR emitter array. This gave us the ability to precisely control and measure damage as a decrease in the photochemical efficiency of PSII using FRRF. Fv/Fm, sigma/σ_{PSII}, and tau were monitored hourly or bihourly to measure the UV damage to PSII relative to non-irradiated conditions. Our aim was to test the UVR emitter array to identify break points in photochemical efficiency, as measured by FRRF, to better understand the physiological constraints of an ecologically important phytoplankton to UVR exposure. Furthermore, we aimed to characterize the transcriptomic profile of *C.*

hystrix under 0.64 mW/cm^2 UVR intensity to reveal transcriptional responses in the central metabolic pathway, photosynthetic electron transport chain (ETC), and DNA repair mechanisms. This study thereby provides a comprehensive investigation of the physiological and molecular stress response to UV irradiation using a UV emitter array designed specifically to dose planktonic phototroph cultures with any desired UVR intensity. These tools and methods, if shown to be successful, could be used to manipulate organisms to better understand how they protect themselves against DNA damage.

Materials and Methods:

Cell Cultures

Corethron hystrix CCMP 308 (Bigelow Laboratory for Ocean Sciences, East Boothbay, Maine, USA) was grown at a maintenance temperature of 14 ºC under 12:12 L:D at an illumination of ~40 µmol photons m^{-2} s^{-1} using white LEDs. Although 14 ºC was the recommended temperature for *in vitro* studies, *C. hystrix* has a much wider known temperature range. Duplicate cultures were grown in L1 medium (Guillard and Hargraves 1993), prepared with 0.2 µm filtered surface seawater from the Gulf of Maine (Bigelow Laboratory for Ocean Sciences, East Boothbay, Maine, USA). Chlorophyll pigment was extracted in 90% acetone at -20 ºC for 17 hours, in the dark. Following extraction, fluorescence of each sub-sample was measured using a 10AU Fluorometer (Turner Designs, Sunnyvale, CA, USA), and chlorophyll concentrations were calculated. Cell counts were determined using a Sedgewick chamber under bright light. Specific growth rates of culture replicates were estimated from the growth curves constructed from chlorophyll *a* fluorescence and cell counts obtained under non-irradiating conditions.

Growth rate (units of doublings per day) was calculated from log-normalized exponential growth phase. Growth curves were used to determine the mid-exponential phase when UVR irradiation would be performed. During the UVR experiments, chlorophyll *a* measurements and morphological cell counts were also collected bihourly in order to changes affected by UVR.

Photosynthetic Kinetics

Fv/Fm, sigma, and tau measurements were monitored using a FRRF (Soliense, Inc, Shoreham, NY, USA). Cell cultures, in biological duplicate, were subjected to either bright white light only at ~ 40 µmol m^{-2} sec^{-1} (control condition) or a combination of bright white light (~ 40 µmol m^{-2} sec^{-1}) and UVR exposure ranging from 0.32 mW/cm^2 to 1.59 mW/cm^2 (experimental condition). UVR was performed using an LED emitter platform (Lumenautix Inc., Reno, NV, USA; Supplementary Fig. S1). The overall experimental period consisted of both control and experimental conditions running for six hours, followed by a dark period of six hours for the two conditions.

NEST Configurable Emitter Array

The NEST array is comprised of multiple discrete solid-state emitters operating in two modes, VIS and UV connected to a control unit (Supplemental Text). The output is regulated and temperature compensated for constant current DC – allowing for precise control and stability of light output. Visible LEDs are blue (3), red (3) and white (6) and the UV emitters (3). For this work only the UV and white LEDs were used. The white LED color temperature is 3985K and the output can vary between 4 and 380 µmol m^{-2} sec^{-1}.

125 The LED array allows for the precise and repeatable incremental *in vitro* irradiation
126 of target organisms to determine their protective, mutative, and repair properties as a
127 function of varying levels of specific electromagnetic energy (Supplementary Fig. S1).
128 The energy categories can be adjusted incrementally and independently to affect the
129 organism's biological functions and to stress the organism to evoke specific physiological
130 responses or cause DNA / RNA mutations.

131 Net UVR organism exposure was reported from the emitter array's gross output
132 after subtracting attenuation from surface reflection, transmittance, absorption, and
133 diffusion of the quartz glass container and seawater. This attenuation was approximately
134 25% of the gross emitter output. Data were collected every hour for UVR energy
135 intensities of 0.32 and 0.64 mW/cm^2 (measured at 285 nm, 12 nm FWHM). At higher
136 doses of 0.96 – 1.59 mW/cm^2 (285 nm 12 nm FWHM), measurements were collected
137 every 30 minutes. Raw data were processed and plotted using the ggplot2 package in the
138 R environment (Wickham 2009). Rate constants for both Fv/Fm and sigma were
139 calculated using a linear regression model also using R.

140 *Illumina sequencing and Gene Expression analysis*

141 After photosynthetic kinetic measurements were made, total RNA was extracted
142 immediately in duplicate from cells in the mid-exponential phase of growth directly after
143 UVR exposure (0.64 mW/cm^2, experimental and control cultures), as well as directly
144 after a dark recovery period of six hours (experimental and control cultures), using the
145 Ambion ToTALLY RNA kit (Life Technologies, Grand Island, NY, USA). The same
146 experimental and control cultures in duplicate were used during both harvesting periods.
147 These extractions produced approximately ~10-12 µg of total RNA from each pellet.

Samples were sent for sequencing at the Biodesign Institute at Arizona State University (Tempe, AZ, USA). Library preparation was fully automated and performed using the Apollo 324 liquid handling platform with selection for polyA RNA. Illumina HiSeq Sequencing yielded 2x100 bp paired-end reads.

Raw sequencing reads were uploaded to the sequencing read archive (NCBI accession: SRP091884, SRX2255404) and inspected using Fastqc (Andrews 2009) to determine quality, ambiguous read percentage and relative amount of sequence reads. Illumina RNA sequencing resulted in an average of 19.4 million raw reads per cDNA library with an average quality score of Q38 (Supplementary Table S1).

Raw Sequencing reads were trimmed using the sequence trimming program Trimmomatic with the following options: Remove any Illumina adapter, cut off the end of any read where the quality score falls below 10, use a sliding window of 5 to cut and trim any base where the average quality score falls below 32 for that window and only keep trimmed reads with a minimum length of 72. (Bolger et al. 2014). De-novo transcript assembly was performed using Velvet (Zerbino and Birney 2008). Optimal k-mer selection, as well as read coverage cutoff selection, was determined by the VelvetOptimiser (Gladman and Seemann 2012). Velvet-constructed contigs were assembled into full-length transcripts using the Oases transcriptome assembler, with a minimum transcript length of 150 base pairs (Schulz et al. 2012). Raw sequences were aligned to the assembled transcripts by Bowtie2 (Langmead and Salzberg 2012). Abundances of mapped sequence reads were calculated using eXpress (Roberts and Pachter 2012), providing the estimated count of reads that mapped to each individual assembled transcript. Estimated counts from eXpress were normalized and counts were

171 calculated using DESeq2 (Love et al. 2014). Transcripts were considered differentially
172 expressed if their associated $\log_2$ fold changes were significant at (adjusted) $p<0.05$,
173 based on the Wald test of DESeq2, while controlling for false discovery using the
174 Benjamini-Hochberg Procedure (Love et al. 2014). Based on our experimental design,
175 differential expression was compared between the UVR+white light irradiated cells
176 (experimental treatment – in duplicate) and bright white light only cells (control
177 treatment – in duplicate), directly after the six hour UVR exposure ended and also after a
178 six-hour dark recovery period.

179 *C. hystrix* is not well annotated. In order to artificially reconstruct the pathways in
180 *C. hystrix*, transcripts from our de-novo assembly were *in silico* translated and compared
181 to Uniprot proteins using Hhblits, which is part of the HH-suite software package
182 (Remmert et al. 2011; The UniProt Consortium 2017). Homologous protein homology
183 was inferred from *in silico* translations using hidden Markov model alignments from
184 Hhblits (Soding 2005). Translated transcripts were considered homologs if there was a
185 >90% probability of the translated transcript being a homolog to a Uniprot protein.

186 Subsequent classification of homologous Uniprot proteins into functional
187 annotation groups was performed by grouping Uniprot Ids based on gene ontology
188 (Ashburner et al. 2000; The Gene Ontology Consortium 2017). In the case of
189 supplemental photosynthetic electron transport, gene ontology provided a poor
190 representation of the selected pathway. For this pathway, homologous proteins from the
191 model centric diatom *Thalassiosira pseudonana* were combined with the Uniprot
192 annotations, with the understanding that this organism's annotations may have changed
193 since they were first annotated and uploaded to public databases in 2004 (Armbrust et al.

194 2004). The entire annotated *Thalassiosira pseudonana* photosynthetic electron transport
195 pathway was downloaded from the Kyoto Encyclopedia of Genes and Genomes (KEGG)
196 (Kanehisa and Goto 2000; Kanehisa et al. 2013).
197 Translated transcripts mapping to a homolog were sometimes one of several
198 contigs. To maintain consistent mapping between homologs, transcript contigs were
199 binned by functional annotation after translation. Additionally, in most cases, up and
200 downregulation variation between contigs was small, making expression patterns more
201 evident. However, on occasion, transcripts for the same functional annotation but
202 different loci were both up and downregulated. Because *C. hystrix* does not have an
203 annotated genome, binning by functional annotation produces an expression overview for
204 the homolog, which accounts for transcriptional variability. Binned isoforms were
205 visualized with a box and whisker plot using the ggplot2 package (Wickham 2009). The
206 line in the box represents the median $\log_2$ fold change when combining all the isoforms.
207 The hinges are the 1st and 3rd quartile.
208
209 **Results:**
210 *Chlorophyll A and Cell Counts under laboratory conditions*
211 *C. hystrix* grew at rate of 0.37 doublings per day based on chlorophyll *a*
212 concentration (linear regression equation $y=5.74 + 0.254x$, $r^2=0.991$) (Supplementary
213 Fig. S2a); this was consistent with microscopic cell counts, which produced a growth rate
214 of 0.392 doublings per day (linear regression equation $y=9.70+0.272x$, $r^2 = 0.990$)
215 (Supplementary Fig. S2b). Under UV light of different intensities, chlorophyll *a* content
216 remained relatively constant during the six-hour irradiation period (Supplementary Fig.

S3). Additionally, there was no significant increase in cell growth over the irradiation period. However, light microscopy revealed morphologically altered cells in the UVR exposed cultures compared to control cultures. The percentage of morphologically intact cells was mostly constant for the lower UVR intensity levels (0.32 – 0.64 mW/cm^2), with a small decrease during the last two hours at 0.64 mW/cm^2 (Fig. 1). However, higher intensities (0.96 – 1.59 mW/cm^2) caused a pronounced decrease in the amount of morphologically intact cells, especially during the last two hours of UVR exposure (Fig. 1).

Photosystem II

To monitor the changes in PSII during exposure to UVR, photosynthetic kinetic measurements were recorded for *C. hystrix* using FRRF (Fig. 2). Several photosynthetic parameters were derived from FRRF measurements. First, Fv/Fm empirically represents the maximum quantum yield of PSII (Fig. 2A) (Geider et al. 1993; Kolber and Falkowski 1993). Fv/Fm is a dimensionless parameter representing how efficiently absorbed photons are used for electron flow: a value of 1 represents complete absorbance efficiency and 0 represents no absorbance (Suggett et al. 2009). A second parameter, sigma is a proxy for the product of the optical cross section for PSII (roughly proportional to the number of chlorophyll molecules per PSII), the efficiency of excitation transfer from the antenna to the PSII reaction center and the quantum yield of charge separation (Fig. 2B) (Mauzerall 1986; Oxborough et al. 2012).

Fv/Fm decreased linearly (Supplementary Table S2) with the rate of decay increasing with intensity (Supplementary Fig. S4-S8, Supplementary Tables S3-S7). Conversely, sigma increased linearly with increasing intensity, demonstrating an inverse

240 relationship between sigma and Fv/Fm for all doses of UVR in this study, with sigma
241 increasing and Fv/Fm decreasing as damage accumulated (Fig. 2 AB, Supplementary Fig.
242 S4-S8). At the higher UVR intensities there was a notable decrease in sigma as
243 photosynthesis became inhibited (Supplementary Table S2). Overall, UVR had a
244 powerful effect on the fluorescence kinetics of PSII, especially at the higher UVR
245 intensities (0.96 – 1.59 mW/cm^2) (Fig. 2, Supplementary Tables S5-S7). For example,
246 sigma increased only 15% from the start of the UVR exposure until the end for the lowest
247 UVR intensity of 0.32 mW/cm^2, with the largest increase evident after three hours under
248 irradiation (Supplementary Fig. S4, Supplementary Table S3). In comparison, at 0.96
249 mW/cm^2, we observed a similar 15% increase in sigma within the first two hours of the
250 start UVR exposure, with a total increase in sigma of approximately 56% over the
251 irradiation period (Supplementary Fig. S6, Supplementary Table S5). Furthermore, UVR
252 intensities of 0.96 mW/cm^2 and 1.28 mW/cm^2 had very strong and similar responses. The
253 rate of change of sigma for each of these two treatments was almost identical and
254 approximately 44% faster than the rate of change observed at 0.64 mW/cm^2
255 (Supplementary Table S2) and 72% faster than the rate observed at 0.32 mW/cm^2. At the
256 highest intensity of 1.59 mW/cm^2, the rate of change for sigma was slower than the rate at
257 0.96 mW/cm^2 and 1.28 mW/cm^2, likely because of extreme damage to the photosynthetic
258 reaction centers.

259 We used RNA-seq to evaluate the expression response of *C. hystrix* PSII
260 transcripts for a single UVR intensity (0.64 mW/cm^2). This intensity was chosen because
261 the majority of cells remained morphologically intact throughout the six-hour irradiation
262 period (Fig. 1). There were 12 differentially expressed PSII related transcripts detected

263 directly after UVR exposure (Fig. 3, Supplementary Fig. S9). All 12 transcripts were
264 downregulated and demonstrated little variation in their fold changes, indicating a strong
265 and coordinated transcriptional response (Fig. 3, Supplementary Fig. S9, Supplementary
266 Table S8). Specific transcripts, related to proteins such as the reaction center core D1 and
267 D2 proteins were significantly downregulated (adjusted $p < 0.001$; Supplementary Table
268 S8), corresponding with observed decreases in the photosynthetic efficiency. Moreover,
269 translated transcripts mapping to cytochrome c550, cytochrome b559 and PSII PsbH
270 proteins were also strongly downregulated.

271 *Reoxidation of the Electron Acceptors*

272 There was very little change in tau 1 during the first 2.5 hours for any dose of
273 UVR (Fig. 2C). After 2.5 hours, turnover time began to increase for the larger UVR
274 doses: 0.96, 1.28, and 1.59 mW/cm^2 (Fig. 2). Overall, tau 1 turnover time increased from
275 26.61 µs at 0.32 mW/cm^2 to 1114.0 µs at 1.28 mW/cm^2 – an approximately 42x increase
276 (Supplementary Table S9). At the highest UVR energy (1.59 mW/cm^2), tau 1 turnover
277 time initially followed the same trend as 1.28 mW/cm^2. However, there was a significant
278 decline in the turnover time after 5 hours (Fig. 2C, Supplementary Table S9), likely
279 because of a severe inhibition in photosynthesis.

280 Tau 2 reacted similarly to tau 1 during UVR exposure, although turnover time for
281 tau 2 was much longer, on the order of milliseconds instead of microseconds (Fig. 2D).
282 For the first two hours of irradiation, there was no significant change in the turnover rate
283 for tau 2 (Fig. 2D). After 2.5 hours, tau 2 increased with each successive increase in UVR
284 energy, with the exception of 1.59 mW/cm^2, which decreased after 5 hours, similar to the
285 behavior of tau 1 for the same treatment (Fig. 2D, Supplementary Table S10).

286 Photosynthetic electron transport genes are not well annotated in the Uniprot
287 database. Thus, proteins from the ubiquitous model centric diatom *T. pseudonana* were
288 combined with available Uniprot proteins to test for electron transport protein homology,
289 as the majority of the photosynthetic electron transport pathway is partially annotated by
290 KEGG (Kanehisa and Goto 2000; Kanehisa et al. 2013). Comparative transcriptomics for
291 the supplemental electron transport pathway of the Z scheme at 0.64 mW/cm^2 were
292 similar to the observations of PSII gene expression. There were 10 transcripts related to
293 supplemental electron transport, most of which are a subunit of the cytochrome b_6f
294 complex. Cytochrome f (*petA*), the largest subunit of the cytochrome b_6f complex (Gray
295 1992), was downregulated according to both our *T. pseudonana* custom database and
296 Uniprot database. Differential expression analysis of the 10 transcripts show nine
297 decreased in abundance and one increased, demonstrating a coordinated downregulation
298 of the supplemental electron transport genes. These results are corroborated by the
299 increases in tau 1 and tau 2 turnover times (0.64 mW/cm^2).

300 *Photosystem I and RuBisCO*

301 Photosynthetic kinetic measurements for photosystem I (PSI) are not reported in
302 this study because they are outside the resolution of the current FRRF machine. However,
303 gene expression of PSI genes was analyzed for the 0.64 mW/cm^2 UVR treatment (Fig. 3).
304 There were 16 PSI related transcripts; 15 transcripts decreased in abundance compared to
305 non-irradiated samples after UVR exposure. Both *psaA* (Apoprotein A1) and *psaB*
306 (Apoprotein A2), which bind through hydrophobic interactions to form the core complex
307 of PSI (Falkowski and Raven 2007) were downregulated under UVR. Additionally, psaD
308 (PSI subunit II) transcripts, which facilitate the docking of ferredoxin and are an essential

309 component of correct PSI function, were downregulated (Hou et al. 2017). Inorganic
310 carbon fixation involves the ribulose-1,5-bisphosphate carboxylase/oxygenase enzyme
311 (RuBisCO). Five transcripts that map to RuBisCO related proteins were downregulated
312 compared to the non-irradiated samples.

313 *Light Harvesting Complex*

314 Light harvesting complexes are photosynthetic protein complexes that harvest
315 light energy and channel it into the PSII and PSI reaction centers. In contrast to the
316 downregulation of PSII and PSI proteins, several light harvesting complex transcripts
317 were upregulated in response to UVR. There was a total of 39 transcripts that mapped to
318 light harvesting related proteins (Fig. 3, Supplementary Table S8). Approximately 54%
319 (21/39) of those transcripts were decreased in abundance compared to the non-irradiated
320 samples, including the highly conserved PSII CP43 and CP47 proteins.

321 *Metabolic Pathway Expression*

322 Glycolytic regulation in plants is accomplished by three main proteins:
323 hexokinase, phosphofructokinase and pyruvate kinase (Plaxton 1996). From the
324 glycolysis pathway, there were 24 differentially expressed transcripts mapping to eight
325 homologous Uniprot proteins. In general, glycolytic Uniprot homologous transcripts
326 showed mixed expression. Three *in silico* translated transcripts mapping to homologous
327 proteins phosphofructokinase, phosphoglycerate kinase and enolase decreased in
328 abundance directly after UVR exposure. Five *in silico* transcripts mapping to homologous
329 proteins aldolase, triosephosphate isomerase, G3P dehydrogenase, phosphoglycerate
330 mutase, and pyruvate kinase increased in abundance directly after UVR exposure (Fig. 4,
331 Supplementary Table S11). None of the transcripts in our data mapped to hexokinase

homologs based on the results from both HMM protein detection and BLASTX (Camacho et al. 2009).

In the tricarboxylic acid (TCA) cycle, we observed 14 differentially expressed *in silico* translated transcripts mapping to 5 homologous Uniprot proteins in the TCA cycle (Supplementary Table S12). The rate limiting step of the TCA cycle, isocitrate dehydrogenase, increased in abundance compared to non-irradiated cells, however the variability between individual transcript expression was very large (Fig. 5). Similar to the transcriptomic results observed in the glycolytic pathway, the overall expression of the TCA cycle was mixed with the same number of up and downregulated transcripts (Fig. 5, Supplementary Table S12).

DNA Repair

There were 70 DNA repair transcripts that were differentially expressed after UVR radiation based on ontological mappings (Supplementary Table S13). Out of those transcripts, 64% (45/70) were decreased in abundance compared to the non-irradiated cells (Fig. 6). Transcripts that increased in abundance were related to recombinational DNA repair. Nine *in silico* translated transcripts mapped to *RecA* homologs (Fig. 6), all of which were increased in abundance, including a transcript with a log2 fold change of 8.04 (256-fold increase) – the largest increase in abundance from the DNA repair pathway over non-irradiated cells. There is also an upregulated transcript related to a photolyase homolog, an enzyme that plays a crucial role in UV-induced DNA repair.

Preliminary Recovery

Following UVR exposure, we conducted a dark recovery period of 6 hours and measured the transcriptional response. In contrast to the results seen directly after UVR

exposure and cellular damage, transcripts in the auxiliary metabolic pathways greatly increased in abundance after dark recovery (Fig. 3-6, Supplementary Tables S14-S17). Approximately 90% of the translated transcripts that mapped to homologous glycolytic and TCA cycle pathway homologs increased their abundance, even after a short dark recovery period of 6 hours. Many transcripts produced $\log_2$ fold changes greater than two, with several greater than $\log_2$ of seven. Furthermore, we observed a notable increase in the amount of DNA repair proteins that were upregulated after dark recovery (Fig. 6). After UVR exposure, approximately 36% of the DNA repair transcripts were increased in abundance compared to the non-irradiated cells; however, after dark recovery that number increased to approximately 76% of the transcripts. It was also observed that transcripts that were increased in abundance directly after irradiation seemed to further increase their abundance after dark recovery.

Discussion:

Controlled laboratory studies describing the impact of UVR on phytoplankton have the potential to improve our understanding of photosynthetic damage and repair as well as general DNA damage and repair. To develop a controlled laboratory methodology for studying the impacts of UVR on photosynthetic and metabolic pathways, we developed a UV light emitter to deliver repeatable doses at a high resolution across a wide spectrum of intensities to monitor for break points in photochemical efficiency using FRRF. To test our emitter array, we selected a cosmopolitan open-ocean diatom, of which members of its genus are found in the Southern Ocean where seasonal UV intensity is high due to ozone depletion. For example, during the spring, pennate and centric diatoms comprise a large portion of the Southern Ocean biomass, and the genus

Corethron is one of the top four genera (Vincent 1988). We chose the diatom *C. hystrix* for our study.

Growth Rate and Cell Morphology

The growth rate for laboratory grown *C. hystrix* under normal photosynthetically active radiation (PAR, ~40 µmol m^{-2} s^{-1}) conditions was similar to published values for several diatoms under analogous light levels (Gilstad and Sakshaug 1990). Higher level plants, which can maintain chlorophyll levels during UVR exposure, may have a higher tolerance to UVR stress as they are able to more efficiently transfer their excitation energy into PSII reaction center proteins (Bornman and Vogelmann 1991; Greenberg et al. 1997). Chloroplast morphology was indeed altered at UVR levels of 0.96-1.59 mW/cm^2, however the largest decrease in intact chloroplasts occurred mostly during the last two hours of irradiation as result of the cumulative UVR dose. Morphological alterations consisted of jagged chloroplasts that migrated toward the center of the cell, which could be a response similar to the "chloroplast clumping" phenomenon seen in other organisms as a form of UV protection (Sharon et al. 2011).

Photosynthetic Kinetics and Gene Expression

Photosystem II damage was affected by both UVR intensity and time during our study, with damage from the highest irradiation treatments ultimately resulting in a loss of photosynthetic function – Fv/Fm becomes approximately zero (Fig. 2A, Supplementary Fig. S4-S8). The observed decrease in Fv/Fm is likely caused by UVR directly damaging PSII reaction centers while also increasing *C. hystrix's* susceptibility to photoinactivation (Rijstenbil 2002). We also observed a corresponding increase in sigma, the functional cross section of PSII which is proportional to the amount of number of

chlorophyll molecules per photosystem II reaction center. This increase may be an environmental adaption to the extreme conditions, where under these conditions, chlorophyll molecules may be transferring their excitation energy away from the damaged reaction centers and into the remaining functional reaction centers, thus increasing the amount of chlorophyll molecules servicing the functional centers and increasing the efficiency of energy transfer of those intact centers.

We observed that UVR intensity begins to have a significant effect on the photosynthetic efficiency and energy transfer by 3 hours at the UV intensity of 0.64 mW/cm^2. These results suggest that the time-dependent damage exceeded repair, provoking an increase in photoinactivation. Furthermore, higher UV intensities (1.28 and 1.59 mW/cm^2) accelerate photoinactivation much more rapidly, because more reaction centers are being irrevocably damaged. The observed decrease in sigma after 3-4 hours (Fig. 2B), for both 1.28 and 1.59 mW/cm^2, indicates that the majority of the reaction centers have been damaged or that chlorophyll can no longer funnel the excitation energy through the functional reaction centers (i.e., a loss of photosynthetic function). Thus, it is clear that photosystem operation is maintained at moderate UVR intensities (0.32-0.96 mW/cm^2) but the cell can only withstand irradiation for several hours before the photosystem is unable to absorb and transfer energy.

For various physiological processes, total dose as compared to dosage rate is important as some changes are the result of a cumulative UVR effect (Frohnmeyer and Staiger 2003; Nawkar et al. 2013). Photosynthetic efficiency (Fv/Fm) decreased twice as fast in cultures irradiated at 1.59 mW/cm^2 than the culture irradiated at 0.64 mW/cm^2. Low Fv/Fm measurements represent a decrease in the efficiency of photosynthesis (i.e.,

424 dynamic photoinhibition), as seen in the coccolithophorid *Emiliania huxleyi* due to high
425 photon flux densities (Critchley 2000; Ragni et al. 2008). Environmental stressors, such
426 as high intensities of photosynthetically active radiation (PAR), adverse temperatures,
427 and water limitation, typically cause photoinhibition. Our decreased Fv/Fm
428 measurements after UVR exposure appear to mimic photoinhibition, which is possibly
429 due to direct damage to PSII by UVR. However, future applications should determine
430 whether molecular changes under a fast damage rate (high cumulative UV dose and rate)
431 are the same as those changes under a more gradual damage rate (high cumulative UV
432 dose but lower rate).

433 Photosystem II is known to be the most sensitive part of the photosynthetic
434 system to UVR exposure, especially the oxygen evolving complex (Post et al. 1996;
435 Szilárd et al. 2007). Our transcriptomic analysis shows that oxygen evolving complex
436 genes, *psbO* (PSII manganese-stabilizing protein), *psbP* (PSII oxygen evolving enhancer
437 protein) and psbV (cytochrome c-550), significantly decreased in abundance. *PsbP* has
438 also been discovered to have a supplemental role in stabilizing the PSII-light harvesting
439 super complexes, with decreasing levels of *psbP* producing a concurrent decrease in the
440 amount of super complexes (Ifuku and Noguchi 2016). We observed that the majority of
441 light harvesting complex transcripts decreased in abundance compared to the non-
442 irradiated controls, especially the CP43 and CP47 related transcripts (Ifuku et al. 2011;
443 Ifuku and Noguchi 2016). The CP47 chlorophyll apoprotein along with its sister protein
444 CP43 are functionally used by the cell to channel the energy from the light harvesting
445 complexes into the reaction center core, (Falkowski and Raven 2007). A previous study
446 observed that both CP47 and CP43 protein expression levels decreased in the

cyanobacteria *Spirulina platensis* during UVR exposure (Rajagopal et al. 2000). Furthermore, the D1 reaction center protein and the aromatic tyrosine electron donors have been shown to be sensitive to UVR (Vass et al. 1996; Bouchard et al. 2006). D1 is one of two main reaction center proteins, while tyrosine amino acids are part of the donor side of PSII absorbing energy at 285 nm, thus making them a possible target for UVR irradiation (Vass et al. 1996). Transcriptome changes demonstrate that both the D1 and D2 reaction center proteins, encoded by *psbA* and *psbB* respectively, mapped to transcripts which decreased in abundance during UVR exposure compared to non-irradiated cells. It has been determined that the overall changes in the expression of *psbA* differ based on the specific organism (Surplus et al. 1998; Huang et al. 2002), however, the decrease in abundance of our *psbA* transcripts during UVR was similar to the changes produced by *Arabidopsis thaliana* (Surplus et al. 1998). Other PSII reaction center transcripts, such as those that mapped to the cytochrome b559 protein, also displayed large decreases in abundance after UVR exposure.

Intuitively, it would be assumed that if these subunits were being actively damaged there would be an increase in their individual gene expression to help mitigate and replace damaged protein subunits. UVR exposure, however, has many other cellular consequences including an increased amount oxidative stress within the cell (Rijstenbil 2002). The Reactive Oxygen Species (ROS) produced during oxidative stress can have serious deleterious effects including photodamage to photosynthetic machinery, an imbalance in the photosynthetic redox signaling pathways and direct inhibition of D1 synthesis, which is necessary for PSII repair (Gururani et al. 2015). The result of these effects is increased photosynthetic photoinhibition. After UVR irradiation, we observed

an upregulation of transcripts related to ATP-dependent Clp proteases and cysteine proteases, chloroplast specific enzymes which play a role in protein turnover, suggesting the cells may indeed be dealing with an increased amount of damaged proteins (Olinares et al. 2011). Additionally, ROS can also activate a signaling cascade, where receptors transmit signals to regulatory molecules which decrease nuclear gene expression of photosynthetic genes (Gururani et al. 2015). This likely explains why nearly complete downregulation of photosynthetic genes is observed for organisms subjected to UVR (Rijstenbil 2002; Gururani et al. 2015).

Tau is a proxy for the PSII reaction center turnover time (Kolber et al. 1988). Both tau 1 and tau 2 turnover times increase significantly at UVR intensities of 0.64-1.59 mW/cm^2 (Fig. 2CD). This is because the plastoquinones QA and QB are directly susceptible to UVR damage (Melis et al. 1992). Our data also illustrate that turnover time corresponds to intensity (Fig. 2C-D, Supplementary Fig. S4-S8, Supplementary Tables S3-S7, S9 and S10). With turnover times increasing up to 0.14 seconds for tau 2 at 1.28 mW/cm^2 (Fig. 2D), these long reoxidation times have a detrimental effect on photosynthesis as excess photon energy causes a buildup of oxidative radicals, thus explaining the genetic downregulation of photosynthetic genes and almost complete loss of photosynthetic function at higher intensities of UVR.

Previously it was observed that the redox state of QA may have an effect on the abundance of light harvesting complex transcript abundances (Maxwell et al. 1995). This phenomenon is perhaps another driving force behind the decrease in abundance in the majority of light harvesting complex transcripts. As the turnover time for QA increases during UVR exposure, the cell may reduce the abundance of certain light harvesting

493 proteins in order to prevent an increase in irradiance stress and higher photoinhibition.
494 Simultaneously, the cell maybe trying to maintain the structural integrity of functional
495 reaction centers (through an increase in chlorophyll binding protein), as a way of limiting
496 damage. This type of competing self-regulation highlights the overall complexity of
497 transcriptomic regulation during UVR exposure.

498 Transcriptome analysis of supplemental photosynthetic electron transport genes
499 corresponds with our PSII expression analysis, as the majority of the transcripts were
500 downregulated compared to the control samples. Most of the transcripts in this subset of
501 data mapped to homologous cytochrome b6-f complex proteins. There are 4 major
502 subunits that make up the cytochrome b6-f complex in algae (Pierre et al. 1995). We
503 identified both of the heme-bearing subunits of the cytochrome b6-f complex, and they
504 were strongly downregulated after UVR exposure. Thus, the cell extends its protective
505 strategy to UVR exposure, using transcriptional downregulation, to complex III in the
506 photosynthetic electron transport chain.

507 Photosystem I is not directly affected by UVR and is more resistant to
508 environmental stressors such as high-light levels (Teramura and Ziska 1996; Zhang et al.
509 2016). However, with an interaction between PSII and PSI due to the photosynthetic
510 electron cascade, UVR exposure will unavoidably have a downstream impact on
511 photosystem I. The transcriptional analysis provided some insight into the health of
512 photosystem I. Of the 16 transcripts from photosystem I, 15 transcripts mapping to four
513 Uniprot homologs, decreased in abundance during irradiation. The majority of the PSI
514 transcripts map to *psaA* and *psaB* which code for PSI P700 chlorophyll *a* apoprotein A1
515 and A2 respectively. *PsaB* binds hydrophobically to *psaA* to form the major reaction

center of PSI (Falkowski and Raven 2007). Additionally, the PSI subunit II (*psaD*) transcripts were also significantly downregulated. *PsaD* is an important protein that is crucial for the stability and correct assembly of PSI while also providing a ferredoxin binding site (Hou et al. 2017). The decreased abundance of *psaA*, *psaB*, and *psaD* transcripts indicates that like PSII and the b_6f complex, transcriptional downregulation was most likely influenced by PSII photoinhibition and oxidative stress, which means it could possibly act as a secondary protective strategy to prevent increased stress and photoinhibition.

The first stage of the photosynthetic dark reactions is the fixation of CO_2 into 3-phosphoglycerate, which is catalyzed by the protein RuBisCO. RuBisCO is the most abundant protein on Earth due to its crucial function combined with its inefficiency as a carboxylase (Raven 2009; Raven 2013). Our data demonstrated a coordinated downregulation for the transcripts mapping to the RuBisCO homologs, with all transcripts decreased in abundance compared to non-irradiated cells (Fig. 3). Previous research on higher order plants demonstrated that UVR exposure caused a large decrease in the activity and expression of RuBisCO when compared to control samples in pea leaves (Strid et al. 1990; Mackerness et al. 1999). Moreover, similar RuBisCO decreases were also observed in jackbean leaves (Choi and Roh 2003). This implies that the mechanism for gene expression decreases in RuBisCO expression ties directly back to the activity of the RuBisCO protein as well as through direct deactivation of its synthesis, similar to these previous studies (Choi and Roh 2003).

Metabolic Pathway Expression

538 UVR exposure is known to cause other metabolic gene expression changes in
539 higher level plants (Jenkins 2009). The glycolytic cycle is the first phase in the
540 catabolism of cellular carbohydrates (Nelson and Cox 2005). The TCA cycle, the second
541 phase of catabolism, is an important source of the cellular reducing agent NADH, which
542 helps generate the proton gradient that is critical for the production of ATP through
543 electron transport (Nelson and Cox 2005). In our study, a coordinated downregulation of
544 transcripts mapping to glycolysis and the TCA cycle was not observed, rather we
545 observed a mixed gene expression pattern directly after UVR exposure (Fig. 4, 5),
546 suggesting that certain enzymes may be shared between multiple pathways for other
547 purposes. Logemann et al. 2000 found that UV-induction of select primary metabolism
548 enzymes that can provide carbon substrates for the shikimate pathway, while Casati et al.
549 2003 discovered that certain primary metabolism enzymes may be induced to provide
550 energy in the form of ATP for the synthesis of molecules necessary for cell survival
551 under UVB stress (Logemann et al. 2000; Casati and Walbot 2003).

552 *DNA Repair*

553 Diatoms are subjected to high doses of UVR in their natural environment
554 (Karentz et al. 1991; Fricke et al. 2011), and the selective pressure of managing UV
555 damage may provide novel insights into mechanisms of DNA repair. Because DNA can
556 directly absorb UVR, the damaged DNA forms cyclobutane pyrimidine dimers (CPDs) or
557 pyrimidine 6-4 photoproducts (6-4PPs) (Sinha and Häder 2002). These photoproducts
558 (i.e., lesions) can cause DNA to make an unnatural conformation, arresting replication
559 (Rastogi et al. 2010). To minimize mutagenic effects, several organisms, including
560 diatoms, produce photoreactivating proteins called photolyases which directly remove the

deleterious dimers (Coesel et al. 2009). Our data demonstrate that a single transcript mapped to a photolyase homolog, and it significantly increased in abundance directly after irradiation (Fig. 6). With its important role in DNA repair, future studies should identify the functional significance for this particular photolyase and how it affects the overall fitness of *C. hystrix* during UVR exposure.

Additionally, there are times where these photoproducts can lead to secondary DNA breaks, or UVR is so intense that double stranded breaks become one of the main photochemical end-products (De Mora et al. 2000). With the emergence of double-stranded breaks, the gene *recA* is recruited to initiate the cellular SOS response, which regulates between 50 and 66 genes involved in double stranded DNA (dsDNA) repair (Smith et al. 1987; Janion et al. 2002). *RecA* mediates homologous recombination repair, which will function to maintain the integrity of DNA. We observed all transcripts mapping to Uniprot *recA* homologs significantly increased in abundance relative to non-irradiated cells (Fig. 6), implicating the activity of these enzymes in dsDNA repair during our study. Furthermore, two site specific DNA-methyltransferase transcripts, which are known to induce the cellular SOS response, were also significantly increased in abundance directly after UVR exposure (Heitman and Model 1987) further highlighting the cells adaption to managing UVR exposure.

Preliminary Recovery

After 6 hours of recovery in dark conditions, several photosynthetic light-harvesting transcripts increased in abundance compared to the non-irradiated samples, with some homologs demonstrating a reversal in expression (Fig. 3, Supplementary Table S14). These results suggest that the cell is possibly trying to repair certain aspects of its

584 UV damaged photosynthetic clusters in order to survive, as photodestruction can cause a
585 complete loss of function for the complex (Lao and Glazer 1996). As the light harvesting
586 complex provides the light energy for the photosystem reaction centers, it would be
587 beneficial for the cell to repair the harvesting complex. Furthermore, homologous
588 transcripts that were part of the cytochrome b6/f complex or maintained roles in
589 photosynthetic electron transport also increased in abundance after night recovery. The
590 largest change in abundance was by a *petF* transcript, which codes for the photosynthetic
591 ferredoxin protein. This expression reversal may indicate that the cells are trying to
592 restart and repair electron transport before PAR light returns to re-energize the
593 photosynthetic system, or that ferredoxin may have a supplemental role in the defense
594 against lingering oxidative stress similar to its response after other biotic attacks (Bilgin
595 et al. 2010).

596 Moreover, despite the tremendous diversity of diatoms, with species estimates
597 ranging from 1×10^4 (Norton et al. 1996) to 2×10^5 (Allen et al. 2006), few studies have
598 focused on the potential biomedical applications of bioactive compounds produced by
599 these organisms (Coesel et al. 2009; Prestegard et al. 2009). There were two polyketide
600 synthetase transcripts which were significantly upregulated after dark recovery (Fig. 6).
601 These enzymes are important in the biosynthesis of many natural products and could be
602 involved in the production of compounds such as mycosporine-like amino acids (MAAs)
603 (Klisch 2008).

604 Still, while there was an upregulation of some transcripts during the dark recovery
605 period, many transcripts especially PSI and II transcripts, were still downregulated after
606 dark recovery (Supplementary Table S14). These results suggest that while the cell is

607 actively trying to repair its photosystem, the damage may have been severe enough that
608 recovery of the whole photosynthetic pathway was not possible during the six-hour
609 recovery period (Neale et al. 1998; Fritz et al. 2008).

610 Our emitter array produced morphological, physiological and molecular responses
611 with extremely high resolution and reproducibility. We demonstrate, based on *C. hystrix*
612 physiological measurements, that our emitter array allowed us to directly manipulate the
613 rate and intensity of photosynthetic damage based on the specific applied UVR energy
614 intensities. We were also able to modulate metabolic gene expression changes. This
615 ability to study specific physiological and molecular responses over a large spectrum of
616 UVR intensities could provide further insights into UV induced damage in other complex
617 organisms. Large-scale screening of organisms that are well adapted to high UV fluxes
618 may contain novel mechanisms or natural compounds, such as photolyases or MAAs,
619 which could increase our understanding of preventive mechanisms and possible
620 treatments resulting from DNA damage.

621

622 **Acknowledgements**

623 We would like to thank Dr. Zbigniew Kolber for his expertise and guidance
624 during the manuscript preparation.

625

626 **Compliance with Ethical Standards**

627 **Conflict of interest**: Authors Robert Read, David Vuono and Iva Neveux declare that
628 they have no conflict of interest. Authors Joseph Grzymski and Carl Staub have a conflict

629 of interest as they are co-founders of the company, EMS Genomics, that developed the

630 light engine.

631

632 **Ethical approval:** This article does not contain any studies with human participants or

633 animals performed by any of the authors.

634 **References:**

635 Allen AE, Laroche J, Maheswari U, Lommer M, Schauer N, Lopez PJ, Finazzi G, Fernie
636 AR, Bowler C (2008) Whole-cell response of the pennate diatom *Phaeodactylum*
637 *tricornutum* to iron starvation. Proc Natl Acad Sci U S A 105:10438–10443. doi:
638 10.1073/pnas.0711370105

639 Allen AE, Vardi A, Bowler C (2006) An ecological and evolutionary context for
640 integrated nitrogen metabolism and related signaling pathways in marine diatoms.
641 Curr Opin Plant Biol 9:264–273. doi: 10.1016/j.pbi.2006.03.013

642 Andrews S (2009) FastQC A Quality Control tool for High Throughput Sequence Data.
643 https://www.bioinformatics.babraham.ac.uk/projects/fastqc/

644 Armbrust EV (2009) The life of diatoms in the world's oceans. Nature 459:185–92.

645 Armbrust EV, Berges JA, Bowler C, Green BR, Martinez D, Putnam NH, Zhou S, Allen
646 AE, Apt KE, Bechner M, Brzezinski MA, Chaal BK, Chiovitti A, Davis AK,
647 Demarest MS, Detter JC, Glavina T, Goodstein D, Hadi MZ, Hellsten U, Hildebrand
648 M, Jenkins BD, Jurka J, Kapitonov VV, Kröger N, Lau WWY, Lane TW, Larimer
649 FW, Lippmeier JC, Lucas S, Medina M, Montsant A, Obornik M, Parker MS,
650 Palenik B, Pazour GJ, Richardson PM, Rynearson TA, Saito MA, Schwartz DC,
651 Thamatrakoln K, Valentin K, Vardi A, Wilkerson FP, Rokhsar DS (2004) The
652 genome of the diatom T*halassiosira pseudonana*: ecology, evolution, and
653 metabolism. Science 306:79–86. doi: 10.1126/science.1101156

654 Ashburner M, Ball CA, Blake JA, Botstein D, Butler H, Cherry JM, Davis AP, Dolinski
655 K, Dwight SS, Eppig JT, Harris MA, Hill DP, Issel-Tarver L, Kasarskis A, Lewis S,
656 Matese JC, Richardson JE, Ringwald M, Rubin GM, Sherlock G (2000) Gene
657 Ontology: tool for the unification of biology. Nat Genet 25:25–29. doi:
658 10.1038/75556

659 Bender SJ, Durkin CA, Berthiaume CT, Morales RL, Armbrust EV (2014)
660 Transcriptional responses of three model diatoms to nitrate limitation of growth.
661 Front Mar Sci 1:3. doi: 10.3389/fmars.2014.00003

662 Berardesca E, Bertona M, Altabas K, Altabas V, Emanuele E (2012) Reduced ultraviolet-
663 induced DNA damage and apoptosis in human skin with topical application of a
664 photolyase-containing DNA repair enzyme cream: clues to skin cancer prevention.
665 Mol Med Rep 5:570–574. doi: 10.3892/mmr.2011.673

666 Bilgin DD, Zavala JA, Zhu J, Clough SJ, Ort DR, DeLucia EH (2010) Biotic stress
667 globally downregulates photosynthesis genes. Plant Cell Environ 33:1597–1613. doi:
668 10.1111/j.1365-3040.2010.02167.x

669 Bolger AM, Lohse M, Usadel B (2014) Trimmomatic: a flexible trimmer for Illumina
670 sequence data. Bioinformatics 30:2114–2120. doi: 10.1093/bioinformatics/btu170

671 Bornman JF, Vogelmann TC (1991) Effect of UV-B Radiation on leaf optical properties
672 measured with fibre optics. J Exp Bot 42:547–554.

673 Bouchard JN, Roy S, Campbell DA (2006) UVB effects on the photosystem II-D1
674 protein of phytoplankton and natural phytoplankton communities. Photochem
675 Photobiol 82:936–951. doi: 10.1562/2005-08-31-IR-666

676 Camacho C, Coulouris G, Avagyan V, Ma N, Papadopoulos J, Bealer K, Madden TL
677 (2009) BLAST+: architecture and applications. BMC Bioinformatics 10:421–429.
678 doi: 10.1186/1471-2105-10-421

679 Casati P, Walbot V (2003) Gene Expression Profiling in Response to Ultraviolet
680 Radiation in Maize Genotypes with Varying Flavonoid Content. Plant Physiol
681 132:1739–1754. doi: 10.1104/pp.103.022871

682 Choi BY, Roh KS (2003) UV-B Radiation Affects Chlorophyll and Activation of
683 Rubisco by Rubisco Activase in *Canavalia ensiformis* L. Leaves. J Plant Biol
684 46:117–121. doi: 10.1007/BF03030440

685 Coesel S, Mangogna M, Ishikawa T, Heijde M, Rogato A, Finazzi G, Todo T, Bowler C,
686 Falciatore A (2009) Diatom PtCPF1 is a new cryptochrome/photolyase family
687 member with DNA repair and transcription regulation activity. EMBO Rep 10:655–
688 661. doi: 10.1038/embor.2009.59

689 Critchley C (2000) Photoinhibition. In: Raghavendra AS (ed) Photosynthesis A
690 Comprehensive Treatise. Cambridge, UK, pp 264–272

691 Cullen JJ, Lesser MP (1991) Inhibition of photosynthesis by ultraviolet radiation as a
692 function of dose and dosage rate: Results for a marine diatom. Mar Biol 111:183–
693 190. doi: 10.1007/BF01319699

694 De Mora S, Demers S, Vernet M (2000) The effects of UV radiation in the marine
695 environment. Cambridge University Press, Cambridge

696 Domingues N, Matos AR, Marques da Silva J, Cartaxana P (2012) Response of the
697 diatom *Phaeodactylum tricornutum* to photooxidative stress resulting from high light
698 exposure. PLoS ONE 7:e38162–6. doi: 10.1371/journal.pone.0038162

699 Dyhrman ST, Jenkins BD, Rynearson TA, Saito MA, Mercier ML, Alexander H,
700 Whitney LP, Drzewianowski A, Bulygin VV, Bertrand EM, Wu Z, Benitez-Nelson
701 C, Heithoff A (2012) The transcriptome and proteome of the diatom *Thalassiosira*
702 *pseudonana* reveal a diverse phosphorus stress response. PLoS ONE 7:e33768. doi:
703 10.1371/journal.pone.0033768

704 Emanuele E, Altabas V, Altabas K, Berardesca E (2013) Topical application of
705 preparations containing DNA repair enzymes prevents ultraviolet-induced telomere
706 shortening and c-FOS proto-oncogene hyperexpression in human skin: an
707 experimental pilot study. J Drugs Dermatol 12:1017–1021.

708 Falkowski PG, Raven JA (2007) Aquatic Photosynthesis, 2nd edn. Princeton

709 Fricke A, Molis M, Wiencke C, Valdivia N, Chapman AS (2011) Effects of UV radiation
710 on the structure of Arctic macrobenthic communities. Polar Biol 34:995–1009. doi:
711 10.1007/s00300-011-0959-4

712 Fritz JJ, Neale PJ, Davis RF, Peloquin JA (2008) Response of Antarctic phytoplankton to
713 solar UVR exposure: inhibition and recovery of photosynthesis in coastal and pelagic
714 assemblages. Mar Ecol Prog Ser 365:1–16. doi: 10.3354/meps07610

715 Frohnmeyer H, Staiger D (2003) Ultraviolet-B radiation-mediated responses in plants.
716 Balancing damage and protection. Plant Physiol 133:1420–1428. doi:
717 10.1104/pp.103.030049

718 Geider RJ, Greene RM, Kolber Z, MacIntyre HL, Falkowski PG (1993) Fluorescence
719 assessment of the maximum quantum efficiency of photosynthesis in the western
720 North Atlantic. Deep-Sea Res Pt I 40:1205–1224. doi: 10.1016/0967-0637(93)90134-
721 o

722 Gilstad M, Sakshaug E (1990) Growth rates of ten diatom species from the Barents Sea at
723 different irradiances and day lengths. Mar Ecol Prog Ser 64:169–173. doi:
724 10.3354/meps064169

725 Gladman S, Seemann T (2012) VelvetOptimiser: automate your Velvet assemblies.
726 https://github.com/tseemann/VelvetOptimiser

727 Gray JC (1992) Cytochrome f: Structure, function and biosynthesis. Photosynth Res
728 34:359–374. doi: 10.1007/BF00029811

729 Greenberg B, Wilson M, Huang X-D, Duxbury C, Gerhardt K, Gensemer R (1997) The
730 effects of ultraviolet-B radiation on higher plants. In: Plants for Environmental
731 Studies. CRC Press, pp 1–35

732 Guillard RRL, Hargraves PE (1993) *Stichochrysis immobilis* is a diatom, not a
733 chrysophyte. Phycologia 32:234–236.

734 Gururani MA, Venkatesh J, Tran L-SP (2015) Regulation of Photosynthesis during
735 Abiotic Stress-Induced Photoinhibition. Molecular Plant 8:1304–1320. doi:
736 10.1016/j.molp.2015.05.005

737 Heitman J, Model P (1987) Site-specific methylases induce the SOS DNA repair
738 response in Escherichia coli. J Bacteriol 169:3243–3250.

739 Helbling EW, Chalker BE, Dunlap WC, Holm-Hansen O, Villafañe VE (1996)
740 Photoacclimation of antarctic marine diatoms to solar ultraviolet radiation. J Exp Mar
741 Bio Ecol 204:85–101. doi: 10.1016/0022-0981(96)02591-9

742 Herbstová M, Bína D, Koník P, Gardian Z, Vácha F, Litvín R (2015) Molecular basis of

743 chromatic adaptation in pennate diatom *Phaeodactylum tricornutum*. BBA-
744 Bioenergetics 1847:534–543. doi: 10.1016/j.bbabio.2015.02.016

745 Hou HJM, Najafpour MM, Moore GF, Allakhverdiev SI (eds) (2017) Photosynthesis:
746 Structures, mechanisms, and applications. Springer International Publishing, Cham

747 Huang L, McCluskey MP, Ni H, LaRossa RA (2002) Global gene expression profiles of
748 the cyanobacterium *Synechocystis* sp. strain PCC 6803 in response to irradiation with
749 UV-B and white light. J Bacteriol 184:6845–6858. doi: 10.1128/JB.184.24.6845-
750 6858.2002

751 Ifuku K, Ido K, Sato F (2011) Molecular functions of PsbP and PsbQ proteins in the
752 photosystem II supercomplex. J Photochem Photobiol B: Biol 104:158–164. doi:
753 10.1016/j.jphotobiol.2011.02.006

754 Ifuku K, Noguchi T (2016) Structural coupling of extrinsic proteins with the oxygen-
755 evolving center in photosystem II. Front Plant Sci 7:121–11. doi:
756 10.3389/fpls.2016.00084

757 Janion C, Sikora nee Wójcik A, Nowosielska A, Grzesiuk E (2002) Induction of the SOS
758 response in starved *Escherichia coli*. Environ Mol Mutagen 40:129–133. doi:
759 10.1002/em.10094

760 Jenkins GI (2009) Signal transduction in responses to UV-B radiation. Annu Rev Plant
761 Biol 60:407–431. doi: 10.1146/annurev.arplant.59.032607.092953

762 Kanehisa M, Goto S (2000) KEGG: kyoto encyclopedia of genes and genomes. Nucleic
763 Acids Res 28:27–30.

764 Kanehisa M, Goto S, Sato Y, Kawashima M, Furumichi M, Tanabe M (2013) Data,
765 information, knowledge and principle: back to metabolism in KEGG. Nucleic Acids
766 Res 42:D199–D205. doi: 10.1093/nar/gkt1076

767 Karentz D, Cleaver JE, Mitchell DL (1991) Cell survival characteristics and molecular
768 responses of antarctic phytoplankton to ultraviolet-b radiation. J Phycol 27:326–341.
769 doi: 10.1111/j.0022-3646.1991.00326.x

770 Klisch M (2008) Mycosporine-like amino acids and marine toxins - the common and the
771 different. Mar Drugs 6:147–163. doi: 10.3390/md20080008

772 Kolber Z, Falkowski PG (1993) Use of active fluorescence to estimate phytoplankton
773 photosynthesis in situ. Limnol Oceanogr 38:1646–1665. doi:
774 10.4319/lo.1993.38.8.1646

775 Kolber Z, Zehr J, Falkowski P (1988) Effects of growth irradiance and nitrogen limitation
776 on photosynthetic energy conversion in photosystem II. Plant Physiol 88:923–929.

777 Kolber ZS, Prášil O, Falkowski PG (1998) Measurements of variable chlorophyll

778 fluorescence using fast repetition rate techniques: defining methodology and
779 experimental protocols. BBA 1367:88–106. doi: 10.1016/s0005-2728(98)00135-2

780 Langmead B, Salzberg SL (2012) Fast gapped-read alignment with Bowtie 2. Nat
781 Methods 9:357–359. doi: 10.1038/nmeth.1923

782 Lao K, Glazer AN (1996) Ultraviolet-B photodestruction of a light-harvesting complex.
783 Proc Natl Acad Sci U S A 93:5258–5263.

784 Ligowski R, Jordan RW, Assmy P (2012) Morphological adaptation of a planktonic
785 diatom to growth in Antarctic sea ice. Mar Biol 159:817–827. doi: 10.1007/s00227-
786 011-1857-6

787 Logemann E, Tavernaro A, Schulz W, Somssich IE, Hahlbrock K (2000) UV light
788 selectively coinduces supply pathways from primary metabolism and flavonoid
789 secondary product formation in parsley. Proc Natl Acad Sci U S A 97:1903–1907.

790 Lohman KE (1960) The ubiquitous diatom–a brief survey of the present state of
791 knowledge. Am J Sci A 258:180–191.

792 Love MI, Huber W, Anders S (2014) Moderated estimation of fold change and dispersion
793 for RNA-seq data with DESeq2. Genome Biol 15:550. doi: 10.1186/s13059-014-
794 0550-8

795 Mackerness S, Jordan BR, Thomas B (1999) Reactive oxygen species in the regulation of
796 photosynthetic genes by ultraviolet-B radiation (UV-B: 280–320 nm) in green and
797 etiolated buds of pea (*Pisum sativum* L.). J Photochem Photobiol B: Biol 48:180–
798 188. doi: 10.1016/s1011-1344(99)00024-x

799 Marchetti A, Schruth DM, Durkin CA, Parker MS, Kodner RB, Berthiaume CT, Morales
800 R, Allen AE, Armbrust EV (2012) Comparative metatranscriptomics identifies
801 molecular bases for the physiological responses of phytoplankton to varying iron
802 availability. Proc Natl Acad Sci U S A 109:E317–25. doi: 10.1073/pnas.1118408109

803 Mauzerall D (1986) The optical cross section and absolute size of a photosynthetic unit.
804 Photosynth Res 10:163–170. doi: 10.1007/BF00118279

805 Maxwell DP, Laudenbach DE, Huner N (1995) Redox regulation of light-harvesting
806 complex II and cab mRNA abundance in *Dunaliella salina*. Plant Physiol 109:787–
807 795.

808 Melis A, Nemson JA, Harrison MA (1992) Damage to functional components and partial
809 degradation of photosystem II reaction center proteins upon chloroplast exposure to
810 ultraviolet-B radiation. BBA-Bioenergetics 1100:312–320. doi: 10.1016/0167-
811 4838(92)90487-x

812 Nawkar G, Maibam P, Park J, Sahi V, Lee S, Kang C (2013) UV-Induced Cell Death in
813 Plants. IJMS 14:1608–1628. doi: 10.3390/ijms14011608

814 Neale PJ, Cullen JJ, Davis RF (1998) Inhibition of marine photosynthesis by ultraviolet
815 radiation: Variable sensitivity of phytoplankton in the Weddell-Scotia Confluence
816 during the austral spring. Limnol and Oceanogr 43:433–448. doi:
817 10.4319/lo.1998.43.3.0433

818 Nelson DL, Cox MM (2005) Lehninger Principles of Biochemistry, 4 edn. W. H.
819 Freeman and Company

820 Norton TA, Melkonian M, Andersen RA (1996) Algal biodiversity. Phycologia 35:308–
821 326. doi: 10.2216/i0031-8884-35-4-308.1

822 Olinares PDB, Kim J, van Wijk KJ (2011) The Clp protease system; a central component
823 of the chloroplast protease network. BBA-Bioenergetics 1807:999–1011. doi:
824 10.1016/j.bbabio.2010.12.003

825 Oxborough K, Moore CM, Suggett DJ, Lawson T, Chan HG, Geider RJ (2012) Direct
826 estimation of functional PSII reaction center concentration and PSII electron flux on
827 a volume basis: a new approach to the analysis of Fast Repetition Rate fluorometry
828 (FRRf) data. Limnol Oceanogr Met 10:142–154. doi: 10.4319/lom.2012.10.142

829 Pierre Y, Breyton C, Kramer D, Popot JL (1995) Purification and characterization of the
830 cytochrome b6 f complex from *Chlamydomonas reinhardtii*. J Biol Chem
831 270:29342–29349.

832 Plaxton WC (1996) The organization and regulation of plant glycolysis. Annu Rev Plant
833 Physiol Plant Mol Biol 47:185–214. doi: 10.1146/annurev.arplant.47.1.185

834 Post A, Lukins PB, Walker PJ, Larkum AW (1996) The effects of ultraviolet irradiation
835 on $P680^+$ reduction in PS II core complexes measured for individual S-states and
836 during repetitive cycling of the oxygen-evolving complex. Photosynth Res 49:21–27.
837 doi: 10.1007/BF00029424

838 Prestegard SK, Oftedal L, Coyne RT, Nygaard G, Skjærven KH, Knutsen G, Døskeland
839 SO, Herfindal L (2009) Marine benthic diatoms contain compounds able to induce
840 leukemia cell death and modulate blood platelet Activity. Mar Drugs 7:605–623. doi:
841 10.3390/md7040605

842 Ragni M, Airs RL, Leonardos N, Geider RJ (2008) Photoinhibition of PsII in *Emiliania*
843 *Huxleyi* (Haptophyta) under high light stress: the roles of photoacclimation,
844 photoprotection, and photorepair. J Phycol 44:670–683. doi: 10.1111/j.1529-
845 8817.2008.00524.x

846 Rajagopal S, Murthy SD, Mohanty P (2000) Effect of ultraviolet-B radiation on intact
847 cells of the cyanobacterium *Spirulina platensis*: characterization of the alterations in
848 the thylakoid membranes. J Photochem Photobiol B: Biol 54:61–66. doi:
849 10.1016/S1011-1344(99)00156-6

850 Rastogi RP, Richa, Kumar A, Tyagi MB, Sinha RP (2010) Molecular mechanisms of

ultraviolet radiation-induced DNA damage and repair. J Nucleic Acids 2010:592980–32. doi: 10.4061/2010/592980

Raven JA (2009) Contributions of anoxygenic and oxygenic phototrophy and chemolithotrophy to carbon and oxygen fluxes in aquatic environments. Aquat Microb Ecol 56:177–192. doi: 10.3354/ame01315

Raven JA (2013) Rubisco: still the most abundant protein of Earth? New Phytol 198:1–3. doi: 10.1111/nph.12197

Remmert M, Biegert A, Hauser A, Söding J (2011) HHblits: lightning-fast iterative protein sequence searching by HMM-HMM alignment. Nat Methods 9:173–175. doi: 10.1038/nmeth.1818

Rijstenbil JW (2002) Assessment of oxidative stress in the planktonic diatom *Thalassiosira pseudonana* in response to UVA and UVB radiation. J Plankton Res 24:1277–1288. doi: 10.1093/plankt/24.12.1277

Roberts A, Pachter L (2012) Streaming fragment assignment for real-time analysis of sequencing experiments. Nat Methods 10:71–73. doi: 10.1038/nmeth.2251

Schulz MH, Zerbino DR, Vingron M, Birney E (2012) Oases: robust de novo RNA-seq assembly across the dynamic range of expression levels. Bioinformatics 28:1086–1092. doi: 10.1093/bioinformatics/bts094

Sharon Y, Dishon G, Beer S (2011) The effects of UV radiation on chloroplast clumping and photosynthesis in the seagrass *Halophila stipulacea* grown under high-PAR conditions. Mar Biol 2011:1–6. doi: 10.1155/2011/483428

Shrestha RP, Tesson B, Norden-Krichmar T, Federowicz S, Hildebrand M, Allen AE (2012) Whole transcriptome analysis of the silicon response of the diatom *Thalassiosira pseudonana*. BMC Genomics 13:499. doi: 10.1186/1471-2164-13-499

Sinha RP, Häder D-P (2002) UV-induced DNA damage and repair: a review. Photochem Photobiol Sci 1:225–236. doi: 10.1039/b201230h

Smith KC, Wang TV, Sharma RC (1987) recA-dependent DNA repair in UV-irradiated Escherichia coli. J Photochem Photobiol B: Biol 1:1–11.

Soding J (2005) Protein homology detection by HMM-HMM comparison. Bioinformatics 21:951–960. doi: 10.1093/bioinformatics/bti125

Strid Å, Chow WS, Anderson JM (1990) Effects of supplementary ultraviolet-B radiation on photosynthesis in *Pisum sativum*. BBA 1020:260–268. doi: 10.1016/0005-2728(90)90156-x

Suggett DJ, Moore CM, Hickman AE, Geider RJ (2009) Interpretation of fast repetition rate (FRR) fluorescence: signatures of phytoplankton community structure versus

886 physiological state. Mar Ecol Prog Ser 376:1–19. doi: 10.3354/meps07830

887 Surplus SL, Jordan BR, Murphy AM, Carr JP, Thomas B, Mackerness SAH (1998)
888 Ultraviolet-B-induced responses in *Arabidopsis thaliana*: role of salicylic acid and
889 reactive oxygen species in the regulation of transcripts encoding photosynthetic and
890 acidic pathogenesis-related proteins. Plant Cell Environ 21:685–694. doi:
891 10.1046/j.1365-3040.1998.00325.x

892 Szilárd A, Sass L, Deák Z, Vass I (2007) The sensitivity of Photosystem II to damage by
893 UV-B radiation depends on the oxidation state of the water-splitting complex. BBA
894 1767:876–882. doi: 10.1016/j.bbabio.2006.11.020

895 Teramura AH, Ziska LH (1996) Ultraviolet-B radiation and photosynthesis. In: Baker NR
896 (ed) Photosynthesis and the Environment. Springer Netherlands, Dordrecht, pp 435–
897 450

898 Tevini M, Teramura AH (1989) UV-B EFFECTS ON TERRESTRIAL PLANTS.
899 Photochem Photobiol 50:479–487. doi: 10.1111/j.1751-1097.1989.tb05552.x

900 The UniProt Consortium (2017) UniProt: the universal protein knowledgebase. Nucleic
901 Acids Res 45:D158–D169. doi: 10.1093/nar/gkw1099

902 The Gene Ontology Consortium (2017) Expansion of the Gene Ontology knowledgebase
903 and resources. Nucleic Acids Res 45:D331–D338. doi: 10.1093/nar/gkw1108

904 Vass I, Sass L, Spetea C, Bakou A, Ghanotakis DF, Petrouleas V (1996) UV-B-induced
905 inhibition of photosystem II electron transport studied by EPR and chlorophyll
906 fluorescence. Impairment of donor and acceptor side components. Biochemistry
907 35:8964–8973. doi: 10.1021/bi9530595

908 Verde C, Prisco GD (2012) Adaptation and Evolution in Marine Environments, Volume
909 2: The Impacts of Global Change on Biodiversity. Springer, Berlin/Heidelberg

910 Vincent WF (1988) Microbial ecosystems of Antarctica. Cambridge University Press

911 Wickham H (2009) ggplot2: elegant graphics for data analysis. Springer New York

912 Wu Y, Li Z, Du W, Gao K (2015) Physiological response of marine centric diatoms to
913 ultraviolet radiation, with special reference to cell size. J Photochem Photobiol B:
914 Biol 153:1–6. doi: 10.1016/j.jphotobiol.2015.08.035

915 Zerbino DR, Birney E (2008) Velvet: Algorithms for de novo short read assembly using
916 de Bruijn graphs. Genome Res 18:821–829. doi: 10.1101/gr.074492.107

917 Zhang Z-S, Jin L-Q, Li Y-T, Tikkanen M, Li Q-M, Ai X-Z, Gao H-Y (2016) Ultraviolet-
918 B radiation (UV-B) relieves chilling-light-induced PSI photoinhibition and
919 accelerates the recovery Of CO2 assimilation in cucumber (C*ucumis sativus L.*)
920 leaves. Sci Rep 1–10. doi: 10.1038/srep34455

Figure Legends

Figure 1: Morphologically intact cells during the 6 hour UVB irradiation period. Morphologically intact cells were estimated by bright light microscopy over the 6-hour irradiation period. All counts were collected both the non-irradiated cells and cells under 5 different intensities of UVB (0.32 mW/cm^2 – 1.59 mW/cm^2). Intact cell counts were collected in triplicate every 2 hours with error bars representing the standard deviation between replicated counts.

Figure 2: **A:** Fv/Fm as a measure of the maximum quantum yield of PSII. **B:** Sigma as a proxy for functional cross section and effective target size of the PSII antenna in Å^2 (quanta)$^{-1}$. **C**: Tau 1 turnover time. During every hour at 0.32 mW/cm^2 and 0.64 mW/cm^2, and every half hour at 0.96-1.59 mW/cm^2 the tau 1 turnover time was calculated using Fast Repetition Rate Fluorometry (FRRF). Irradiation time is on the x-axis with the turnover time in µs on the y-axis. **D**: Tau 2 turnover time. During every hour at 0.32 mW/cm^2 and 0.64 mW/cm^2, and every half hour at 0.96-1.59 mW/cm^2 the tau 2 turnover time was calculated using Fast Repetition Rate Fluorometry (FRRF). Irradiation time is on the x-axis with the turnover time in µs on the y-axis. Note the drop in turnover time at 1.28 and 1.59 mW/cm^2.

Figure 3: Metabolic pathway reconstruction of the photosynthetic electron transport chain. Uniprot names for each gene product correspond to heat map subplots in the order shown (left- to-right for condition (directly after UVR and after dark recovery) and top-to-bottom for each Uniprot name). Higher transcript abundance is represented in red

(upregulation), lower transcript abundance in blue (downregulation) and empty spots represent a Uniprot homolog wasn't differentially expressed during that condition.

Figure 4: Box and whisker plot for Uniprot glycolysis homologs. Log_2 fold changes directly after UVR irradiation are represented in the left figure – labeled "Day" – while log_2 fold changes after six-hour dark recovery – labeled "Night" – are represented in the figure to the right. The line within the box is the median of the log_2 fold changes for that specific homolog. The hinges are the 1st and 3rd quartile. The upper whisker starts from the hinge and ends at the highest value that is within 1.5 * inter-quartile range of the hinge. The lower whisker extends form the hinge to the lowest value that is within 1.5 * inter-quartile range. The x-axis is consistent between both figures, therefore some homologs (e.g. Glucose−6−phosphate isomerase – directly after UVR irradiation) will have missing data in their specific figure, as there were no differentially expressed *in silico* translated transcripts mapping to that homolog during that time.

Figure 5: Box and whisker plot for Uniprot TCA homologs. Log_2 fold changes directly after UVR irradiation are represented in the left figure – labeled "Day" – while log_2 fold changes after six-hour dark recovery – labeled "Night" – are represented in the figure to the right. The line within the box is the median of the log_2 fold changes for that specific homolog. The hinges are the 1st and 3rd quartile. The upper whisker starts from the hinge and ends at the highest value that is within 1.5 * inter-quartile range of the hinge. The lower whisker extends form the hinge to the lowest value that is within 1.5 * inter-quartile range. The x-axis is consistent between both figures, therefore some homologs

968 (e.g. Aconitase – directly after UVR irradiation) will have missing data in their specific
969 figure, as there were no differentially expressed *in silico* translated transcripts mapping to
970 that homolog during that time.
971
972 Figure 6: Box and whisker plot for Uniprot DNA repair homologs. Log_2 fold changes
973 directly after UVR irradiation are represented in the left figure – labeled "Day" – while
974 log_2 fold changes after six-hour dark recovery – labeled "Night" – are represented in the
975 figure to the right. The line within the box is the median of the log_2 fold changes for that
976 specific homolog. The hinges are the 1^{st} and 3^{rd} quartile. The upper whisker starts from
977 the hinge and ends at the highest value that is within 1.5 * inter-quartile range of the
978 hinge. The lower whisker extends form the hinge to the lowest value that is within 1.5 *
979 inter-quartile range. The x-axis is consistent between both figures, therefore some
980 homologs will have missing data in their specific figure, as there were no differentially
981 expressed *in silico* translated transcripts mapping to that homolog during that time.

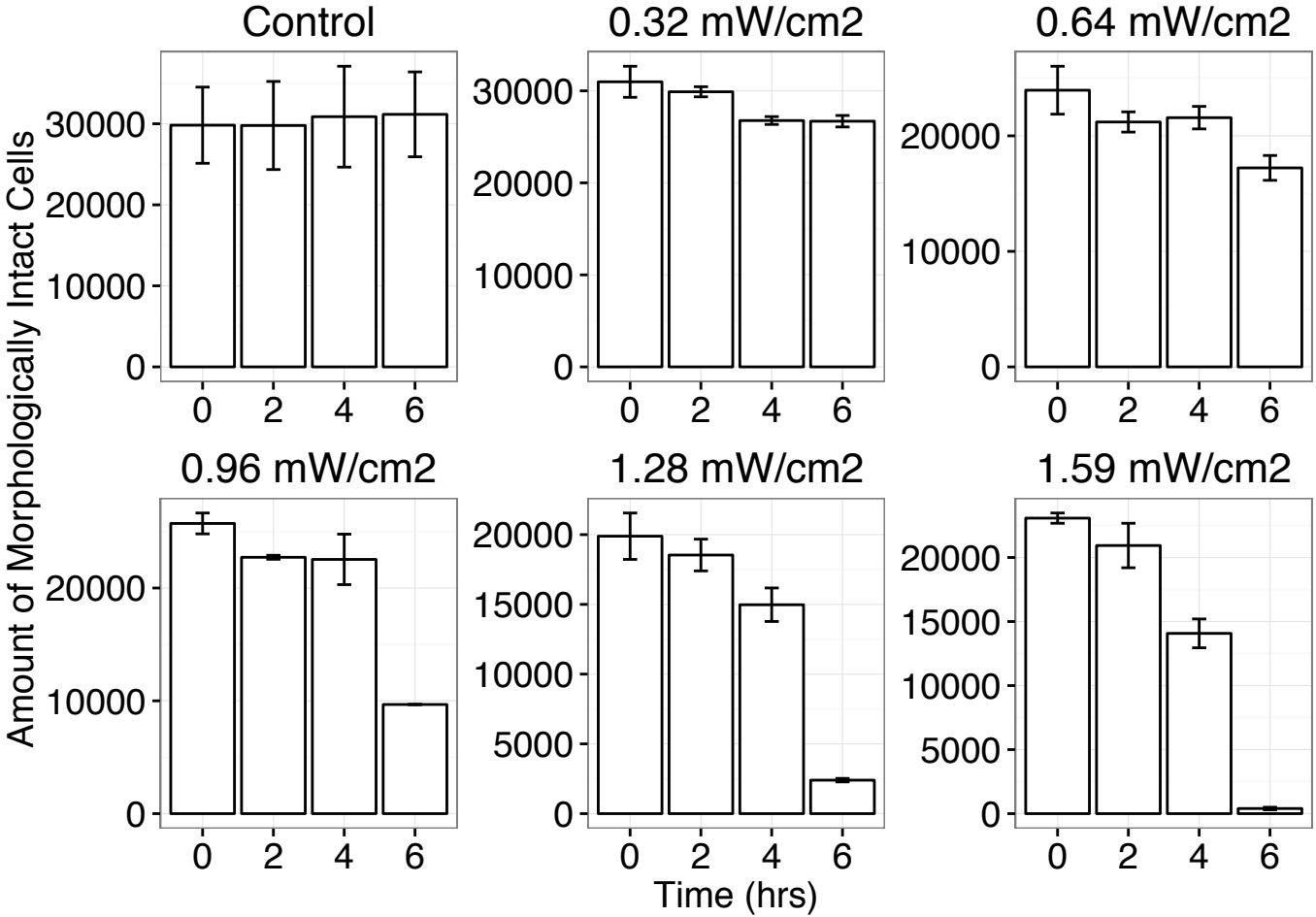
Control
0.32 mW/cm2
0.64 mW/cm2
0.96 mW/cm2
1.28 mW/cm2
1.59 mW/cm2
Amount of Morphologically Intact Cells
Time (hrs)
0
2
4
6
0
10000
20000
30000
5000
15000

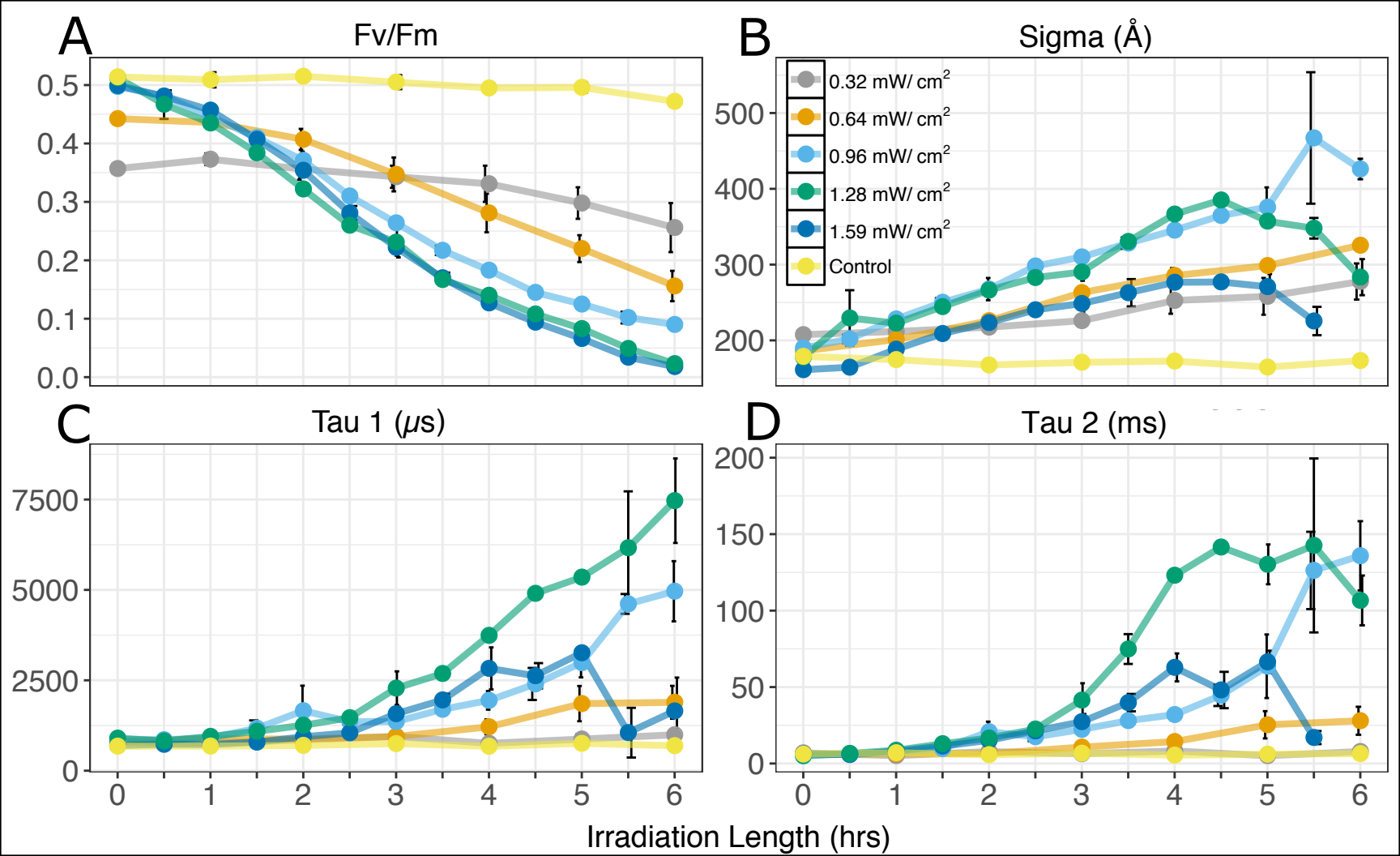
A
Fv/Fm
0.5
0.4
0.3
0.2
0.1
0.0
B
Sigma (Å)
500
400
300
200
0.32 mW/ cm2
0.64 mW/ cm2
0.96 mW/ cm2
1.28 mW/ cm2
1.59 mW/ cm2
Control
C
Tau 1 (μs)
7500
5000
2500
0
D
Tau 2 (ms)
200
150
100
50
0
0
1
2
3
4
5
6
Irradiation Length (hrs)

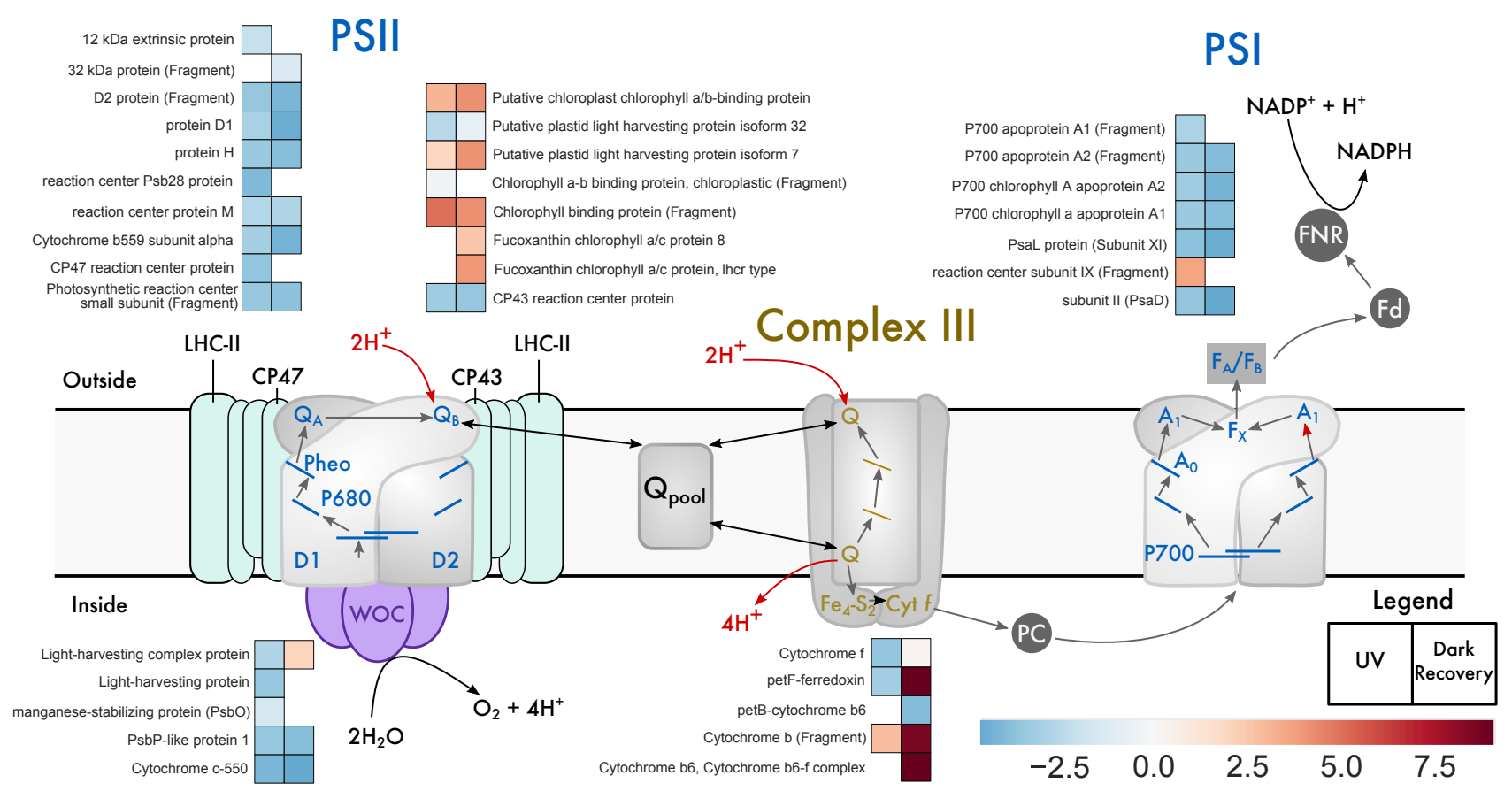
PSII
12 kDa extrinsic protein
32 kDa protein (Fragment)
D2 protein (Fragment)
protein D1
protein H
reaction center Psb28 protein
reaction center protein M
Cytochrome b559 subunit alpha
CP47 reaction center protein
Photosynthetic reaction center small subunit (Fragment)
Putative chloroplast chlorophyll a/b-binding protein
Putative plastid light harvesting protein isoform 32
Putative plastid light harvesting protein isoform 7
Chlorophyll a-b binding protein, chloroplastic (Fragment)
Chlorophyll binding protein (Fragment)
Fucoxanthin chlorophyll a/c protein 8
Fucoxanthin chlorophyll a/c protein, lhcr type
CP43 reaction center protein
PSI
P700 apoprotein A1 (Fragment)
P700 apoprotein A2 (Fragment)
P700 chlorophyll A apoprotein A2
P700 chlorophyll a apoprotein A1
PsaL protein (Subunit XI)
reaction center subunit IX (Fragment)
subunit II (PsaD)
NADP+ + H+
NADPH
FNR
Fd
Complex III
LHC-II
CP47
CP43
LHC-II
Outside
Inside
2H+
2H+
4H+
QA
QB
Pheo
P680
D1
D2
WOC
2H2O
O2 + 4H+
Qpool
Q
Q
Fe4-S2
Cyt f
PC
FA/FB
A1
FX
A1
A0
P700
Light-harvesting complex protein
Light-harvesting protein
manganese-stabilizing protein (PsbO)
PsbP-like protein 1
Cytochrome c-550
Cytochrome f
petF-ferredoxin
petB-cytochrome b6
Cytochrome b (Fragment)
Cytochrome b6, Cytochrome b6-f complex
Legend
UV
Dark Recovery
−2.5
0.0
2.5
5.0
7.5

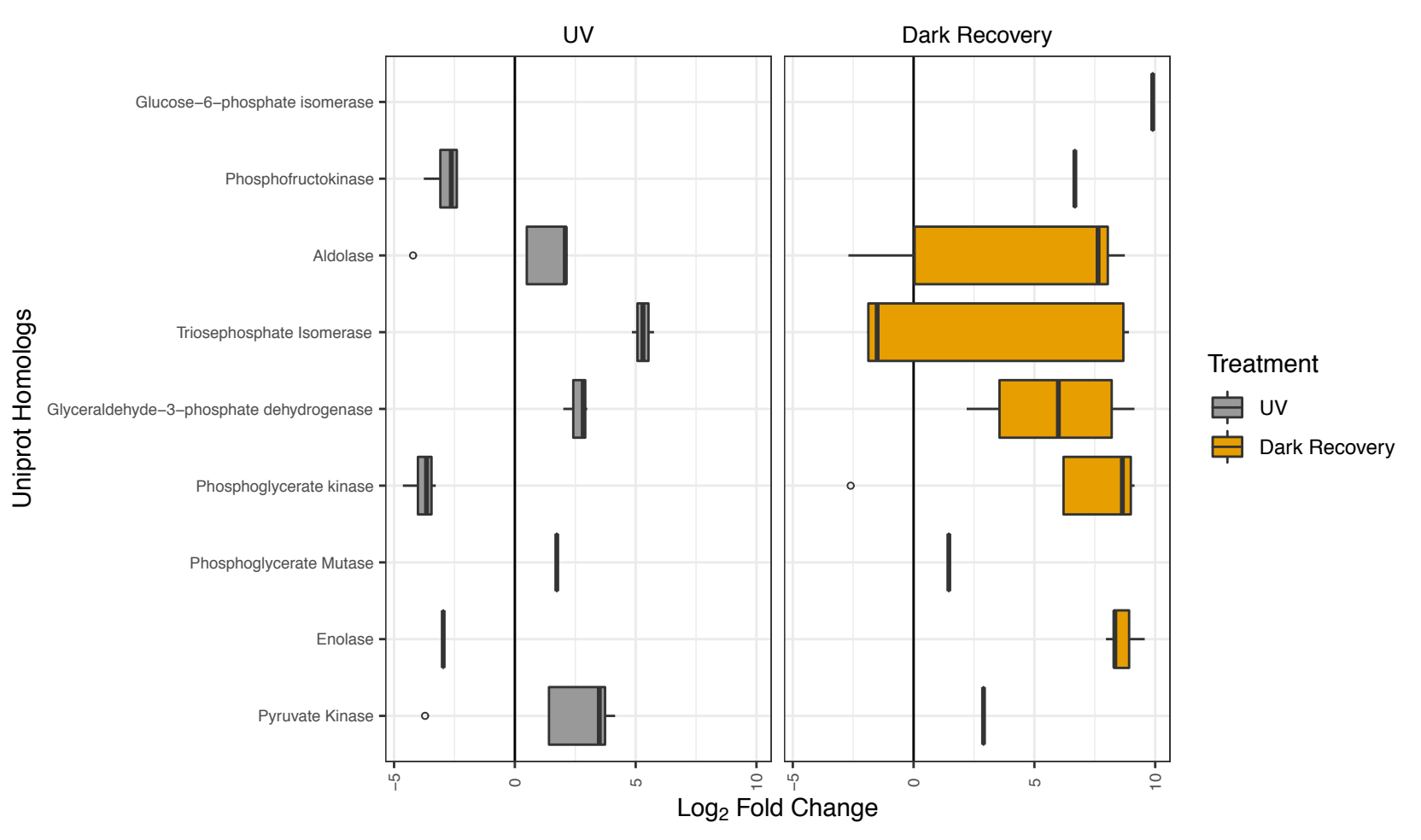
UV
Dark Recovery
Glucose−6−phosphate isomerase
Phosphofructokinase
Aldolase
Triosephosphate Isomerase
Glyceraldehyde−3−phosphate dehydrogenase
Phosphoglycerate kinase
Phosphoglycerate Mutase
Enolase
Pyruvate Kinase
Uniprot Homologs
−5
0
5
10
Log2 Fold Change
Treatment
UV
Dark Recovery

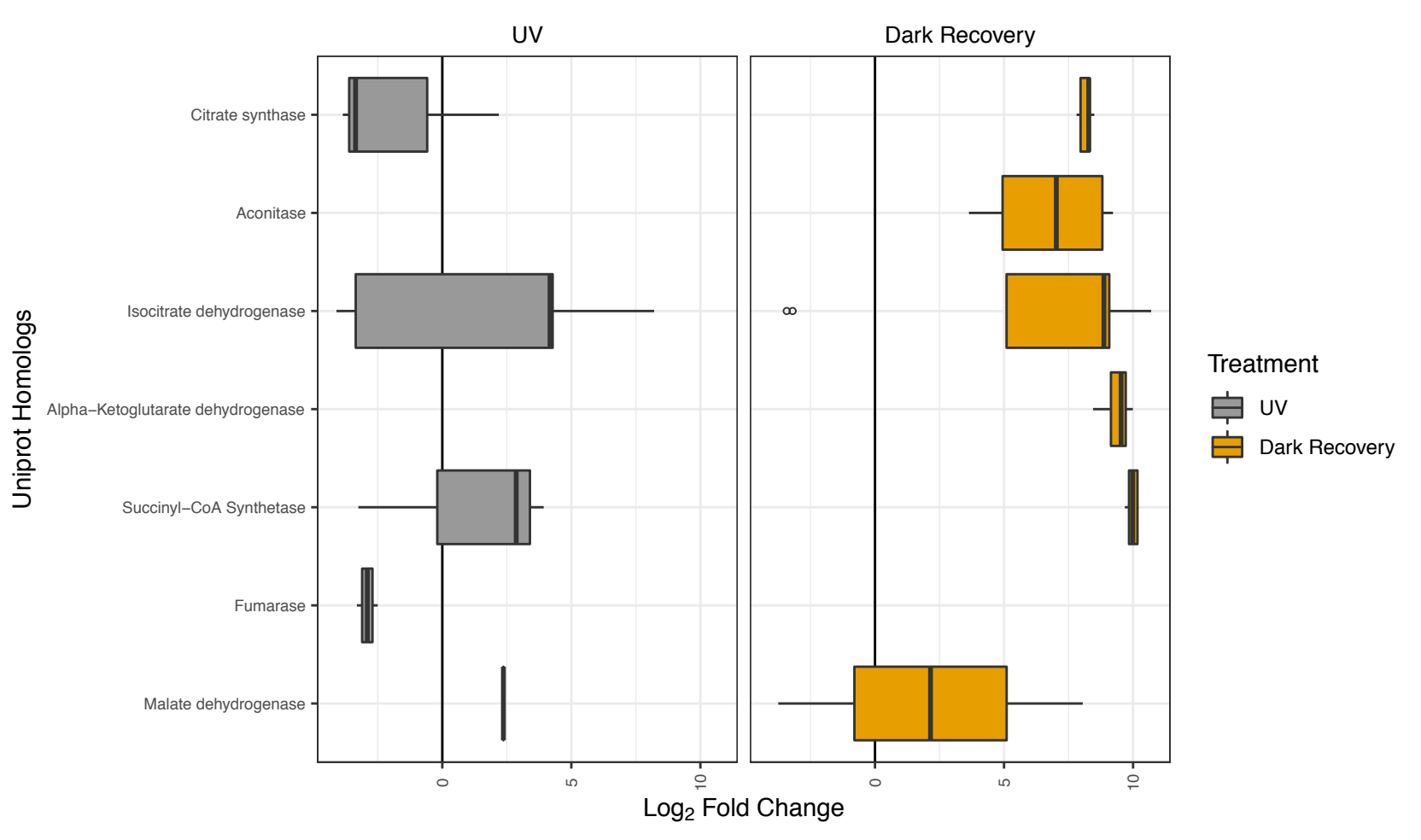
UV
Dark Recovery
Citrate synthase
Aconitase
Isocitrate dehydrogenase
Alpha−Ketoglutarate dehydrogenase
Succinyl−CoA Synthetase
Fumarase
Malate dehydrogenase
Uniprot Homologs
0
5
10
8
Log2 Fold Change
Treatment
UV
Dark Recovery

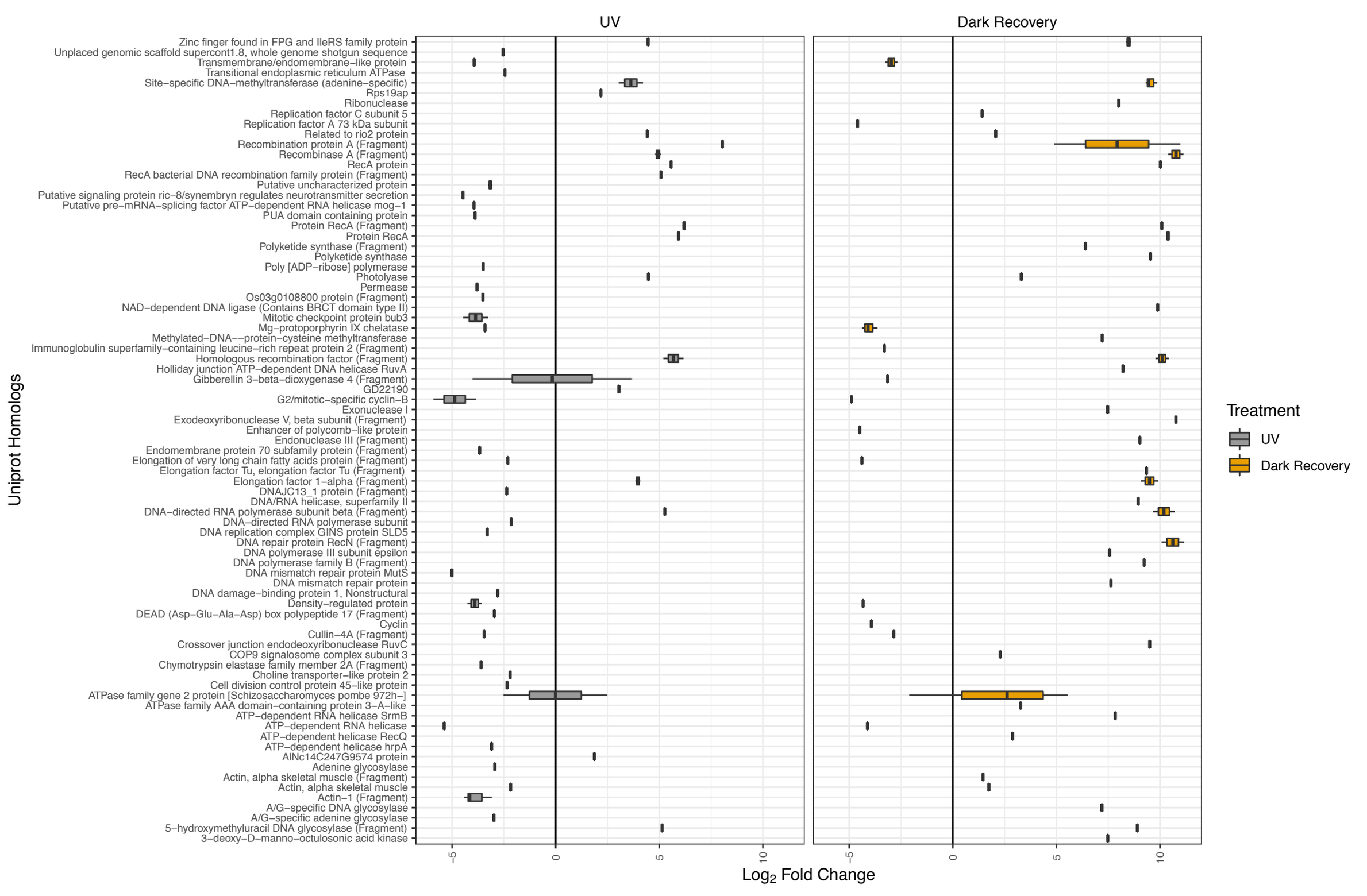
UV
Dark Recovery
Zinc finger found in FPG and IleRS family protein
Unplaced genomic scaffold supercont1.8, whole genome shotgun sequence
Transmembrane/endomembrane−like protein
Transitional endoplasmic reticulum ATPase
Site−specific DNA−methyltransferase (adenine−specific)
Rps19ap
Ribonuclease
Replication factor C subunit 5
Replication factor A 73 kDa subunit
Related to rio2 protein
Recombination protein A (Fragment)
Recombinase A (Fragment)
RecA protein
RecA bacterial DNA recombination family protein (Fragment)
Putative uncharacterized protein
Putative signaling protein ric−8/synembryn regulates neurotransmitter secretion
Putative pre−mRNA−splicing factor ATP−dependent RNA helicase mog−1
PUA domain containing protein
Protein RecA (Fragment)
Protein RecA
Polyketide synthase (Fragment)
Polyketide synthase
Poly [ADP−ribose] polymerase
Photolyase
Permease
Os03g0108800 protein (Fragment)
NAD−dependent DNA ligase (Contains BRCT domain type II)
Mitotic checkpoint protein bub3
Mg−protoporphyrin IX chelatase
Methylated−DNA−−protein−cysteine methyltransferase
Immunoglobulin superfamily−containing leucine−rich repeat protein 2 (Fragment)
Homologous recombination factor (Fragment)
Holliday junction ATP−dependent DNA helicase RuvA
Gibberellin 3−beta−dioxygenase 4 (Fragment)
GD22190
G2/mitotic−specific cyclin−B
Exonuclease I
Exodeoxyribonuclease V, beta subunit (Fragment)
Enhancer of polycomb−like protein
Endonuclease III (Fragment)
Endomembrane protein 70 subfamily protein (Fragment)
Elongation of very long chain fatty acids protein (Fragment)
Elongation factor Tu, elongation factor Tu (Fragment)
Elongation factor 1−alpha (Fragment)
DNAJC13_1 protein (Fragment)
DNA/RNA helicase, superfamily II
DNA−directed RNA polymerase subunit beta (Fragment)
DNA−directed RNA polymerase subunit
DNA replication complex GINS protein SLD5
DNA repair protein RecN (Fragment)
DNA polymerase III subunit epsilon
DNA polymerase family B (Fragment)
DNA mismatch repair protein MutS
DNA mismatch repair protein
DNA damage−binding protein 1, Nonstructural
Density−regulated protein
DEAD (Asp−Glu−Ala−Asp) box polypeptide 17 (Fragment)
Cyclin
Cullin−4A (Fragment)
Crossover junction endodeoxyribonuclease RuvC
COP9 signalosome complex subunit 3
Chymotrypsin elastase family member 2A (Fragment)
Choline transporter−like protein 2
Cell division control protein 45−like protein
ATPase family gene 2 protein [Schizosaccharomyces pombe 972h−]
ATPase family AAA domain−containing protein 3−A−like
ATP−dependent RNA helicase SrmB
ATP−dependent RNA helicase
ATP−dependent helicase RecQ
ATP−dependent helicase hrpA
AlNc14C247G9574 protein
Adenine glycosylase
Actin, alpha skeletal muscle (Fragment)
Actin, alpha skeletal muscle
Actin−1 (Fragment)
A/G−specific DNA glycosylase
A/G−specific adenine glycosylase
5−hydroxymethyluracil DNA glycosylase (Fragment)
3−deoxy−D−manno−octulosonic acid kinase
Uniprot Homologs
−5
0
5
10
Log2 Fold Change
Treatment
UV
Dark Recovery